High-Resolution Electrostatic Analog Tunable Grating With a Single-Mask Fabrication Process

Wei-Chuan Shih, Sang-Gook Kim, *Member, IEEE, ASME, Member*, and George Barbastathis, *Member, IEEE*

***Abstract*—We present the design, modeling, fabrication, and characterization of the microelectromechanical systems (MEMS) analog tunable diffraction grating with the concept of transverse actuation. In contrast to the vertically actuated "digital" tunable grating, our prototype design trades angular tunable range for tuning resolution. The prototype shows an angular tunable range of 250 μrad with 1-μrad resolution at 10 V. Grating pitch changes corresponding to the full range and resolution are 57 nm and 2.28 Å, respectively confirmed by experimental measurement and theoretical calculation. Simulation shows that subradian tunable range is feasible with better lithographic design rules or higher actuation voltage. The single-mask fabrication process offers several advantages: 1) Excellent optical flatness; 2) ease of fabrication; and 3) great flexibility of device integration with existing on-chip circuitry. Tunable gratings such as the one presented here can be used for controlling dispersion in optical telecommunications, sensing, etc., applications. [1611]**

***Index Terms*—Diffraction gratings, electrostatic, fabrication, high resolution, microelectromechanical systems (MEMS), single mask, tunable.**

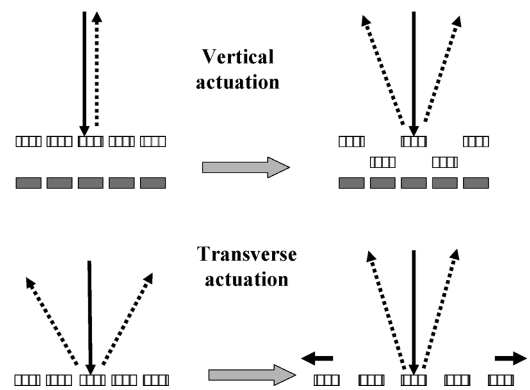

Fig. 1. Schematic diagram of the working concepts of tunable gratings by vertical ("digital") and transverse ("analog") actuation.

I. Introduction

DIFFRACTION gratings are commonly used as dispersive elements in many optical systems. Applications include spectrometers, switching, tuning and thermal compensation (trimming) elements in dense wavelength-division multiplexing (DWDM), visual display technology, external cavity lasers, etc. For dynamic tuning, silicon light machines have commercialized the grating light valve (GLV) [1], [2] as a light modulator. The grating pitch of the GLV is controlled digitally by moving the grating beams in the vertical direction. Sinclair *et al.* demonstrated the polychromator [3] which utilizes a similar actuation principle with control of the beam height to modulate the diffraction efficiency. The angular resolution of these "digital" systems is, however, limited by the minimum beam width. In turn, that is limited by the lithographic resolution. Analog angular tuning, on the other hand, seeks to deliver better resolution by employing the following principles at small scale: 1) Thermal actuation of microelectromechanical systems (MEMS) gratings [4], [5]; 2) thermal and/or magnetic actuation of fiber Bragg gratings [6]; and 3) electrostatic actuation for variable blaze angles [7]. Recently, a different tuning mechanism has been proposed which explored the idea of stretching a grating on the sides using controlled forces offered by MEMS actuators [8], [9]. The transverse actuation changes the pitch, and, therefore, the diffraction angle, in an analog fashion, as shown in Fig. 1. Two embodiments were pursued, namely, through electrostatic and piezoelectric actuation [10]. Electrostatic actuation offers much less force than piezoelectric actuation; therefore, flexure design is necessary for device function. This is likely to lower the structural stiffness as well as mechanical resonant frequency. However, electrostatic actuation is attractive from the viewpoint of: 1) Near residual stress free optical layer; 2) ease of fabrication; and 3) great flexibility of device integration with existing on-chip circuitry. Precise control of the diffraction angle can be achieved by closed-loop operation, which, however, was not implemented in the design presented here. Since the size of the electrostatic device is limited by peak actuation voltage considerations, our analog approach trades angular tunable range for tuning resolution compared to the digital alternatives.

Manuscript received June 7, 2005; revised August 25, 2005. This work was supported by the ASML Holding H. V. Corporation and by Korea Institute of Machinery and Materials (KIMM). Subject Editor O. Solgaard.

The authors are with the Department of Mechanical Engineering, Massachusetts Institute of Technology, Cambridge, MA 02139 USA (e-mail: wshih@mit.edu).

Digital Object Identifier 10.1109/JMEMS.2006.879369

II. Device Design

The device principle and physical parameters are shown schematically in Fig. 2. Two comb-drives [11] pull on both sides of a periodic structure to achieve transverse actuation. The structure is composed of a grating in the center window and flexures which connect each grating period. The flexures are springs which determine the transverse stiffness of the structure. The entire suspended structure is attached to a silicon substrate via four anchors.

A. Structure and Actuator Design

As shown in Fig. 2, two kinds of elements contribute to the compliance of this device: The four supporting beams which

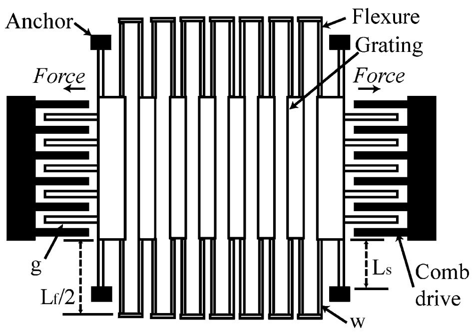

Fig. 2. Top-view schematic diagram showing the working principle and design parameters of the electrostatic analog tunable grating. The grating is connected by flexures to four anchors. Actuation force is offered by comb-drives on both sides. Important design parameters are: Length of the supporting beams (L_s), length of the flexure beams (L_f), width of the flexure (w), and gap between adjacent fingers of the comb-drives (g).

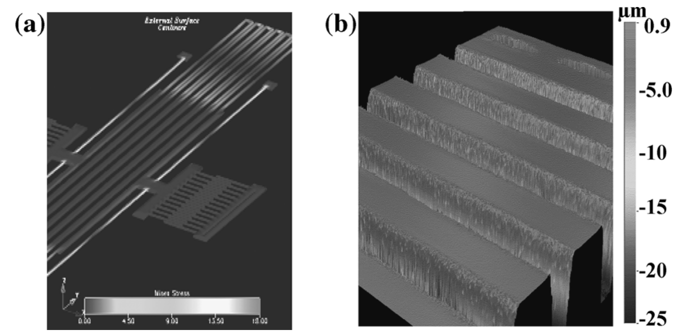

Fig. 3. (a) Simulated stress distribution after 0.6 μN is applied on both sides. Note that the optical grating region is stress free. Stress is in millipascal. (b) Surface quality measured using WYKO, showing excellent optical flatness of this device.

connect the suspended structure to the anchors, and the flexures which connect adjacent grating beams. The stiffness of the supporting beams on one side can be estimated, using a model of two clamped-clamped beams in parallel [12], by

$$k_s = \frac{2Ew^3t}{L_s^3} \tag{1}$$

where k_s is the effective spring constant of the supporting beam, E is the Young's modulus of the material, t is the thickness of the structure, w is the width of the beam, and L_s is the length of the supporting beam. The stiffness of the flexure between two adjacent beams (one grating period) is estimated by

$$k_f = \frac{8Ew^3t}{L_f^3} \tag{2}$$

where L_f is the length of the flexure connecting the grating structure (see Fig. 2). The flexure stiffness is selected based on a tradeoff between the mechanical resonant frequency and the actuation voltage. In other words, the device needs to be compliant enough to have low maximal tuning voltage (~10 V); meanwhile, the device needs to be stiff enough for the resonant frequency to be high.

The driving force is rendered by the two comb-drives on either side. Since electrostatic comb-drives draw essentially negligible current, power consumption is minimized. The disadvantage is that comb-drives deliver small force, usually limited to micronewton or less, depending on the device thickness and the applied voltage. Ignoring edge effects (fringing), the driving force can be estimated by

$$F = \frac{N\varepsilon t}{2g}V^2 \tag{3}$$

where N is the number of finger pairs, ε is the permittivity of air, t is the thickness of the structure, g is the gap distance between two adjacent fingers, and V is the applied voltage.

Since the performance of the device greatly relies on the uniformity of the grating pitch change, we use finite-element analysis (Coventorware, Coventor, NC) to predict the strain distribution across the grating by the transverse actuation. Simulations show that stress concentration is well under the yield stress level and only occurs at the junction of the flexures and the grating beams for the whole tunable range. Therefore, the optical grating can maintain its global periodicity under the assumption of material uniformity. One example of how the stress is distributed within an actuated device is shown in Fig. 3(a).

B. Optical Design

The diffraction angle of a grating at normal incidence under the paraxial approximation is given by the grating equation:

$$\sin\theta = \frac{m\lambda}{p_0} \tag{4}$$

where m is the diffraction order, λ is the wavelength of the incident light (632.8 nm throughout this paper), and p_0 is the pitch of the grating. Expanding the previous equation in a Taylor series for a small pitch change Δp, we find the response angle given by

$$\Delta\theta \cong \frac{m\lambda}{p_0^2}\Delta p. \tag{5}$$

This relationship shows that the maximum tunable range can be greatly increased if a smaller-pitch grating can be fabricated. The minimum grating pitch is set by the resolution of the available lithography tool ("critical dimension"). Since the flexures on the sides of the grating must be defined, we find that the minimum grating pitch is, at best, four times the critical dimension for 75% duty cycle or six times the critical dimension for 50% duty cycle (DC, defined as the ratio of the grating beam width to the pitch). Considering the state-of-the-art integrated circuit (IC) fabrication capability, a grating of 1-μm pitch is not difficult to make. However, the fabrication capability available to us is a minimum linewidth of 2 μm which results in a 12-μm-pitch grating with 50% DC. The maximum tunable range for this design at 10 V is ~0.22 μrad. If the 1-μm-pitch grating can be fabricated, its angular tunable range should be 144 times (~31.7 μrad) larger than the current design at the same applied voltage. On the other hand, if the maximum actuation voltage is

TABLE I
DESIGN PARAMETERS AND DEVICE PERFORMANCE

DESIGN PARAMETERS								
L_s (μm)	L_f (μm)	w (μm)	t (μm)	N	g (μm)	p_0 (μm)	DC (%)	n
450	400	2	2	80	2	12	50	17

SIMULATED PERFORMANCE					
a (rad/V^2)	Efficiency loss (ppm)	Pitch change (nm)	Comb-drive travel (μm)	Tuning range (μrad)	Actuation voltage (V)
$2.156*10^{-6}$	30 (DC=48.3%)	442 (3.7% of p_0)	3.54	1941	30
	<<1 (DC=49.8%)	49.1 (0.4% of p_0)	0.393	215.6	10
EXPERIMENTAL PERFORMANCE					
$2.399x10^{-6}$	0.6% (DC=44%)	57.4 (0.47% of p_0)	0.459	250.5±1	10

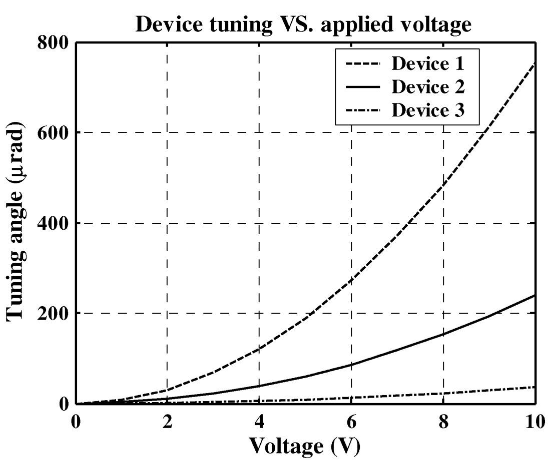

Fig. 4. Angular tuning versus applied voltage simulations. The quadratic response is characteristic to electrostatic comb-drives. Three devices with different flexure designs were simulated. Device 2 is the prototype used in Section IV.

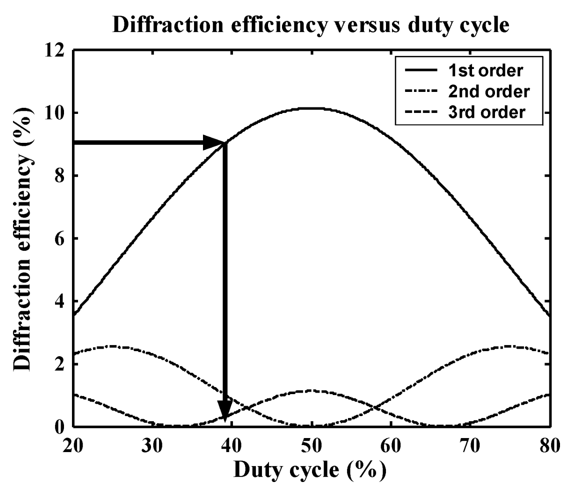

Fig. 5. Diffraction efficiency versus duty cycle (binary amplitude grating) simulation. The arrow points out that the 10% loss of the first-order diffraction efficiency occurs at 39.8% duty cycle.

30 V, the 12-μm-pitch grating has a tunable range of $\sim$1.9 μrad. Therefore, though tunable range is currently not the focus of our research, subradian tunable range is achievable. However, excessive tuning would suffer substantial diffraction efficiency loss, as will evidenced in Fig. 5.

Combining (1)–(5), the expression relating tuning angle to applied voltage is derived

$$\Delta\theta = \frac{N\lambda\varepsilon}{2gp^2Ew^3}\left\{\frac{2}{L_s^3}+\frac{1}{L_f^3}\right\}^{-1}V^2 = aV^2 \qquad (6)$$

where the whole term involving design parameters before voltage squared is lumped as the coefficient a.

Key design parameters, simulation results, and experimental measurements of the device tested are summarized in Table I, and the simulations of tuning angle versus applied voltage for three different flexure designs are shown in Fig. 4. Devices with more compliant flexures, though have larger tunable range, possess lower mechanical resonant frequency.

To achieve high vertical stiffness, we chose to use silicon-on-insulator (SOI) wafers with device layer thickness of 20 μm. Since light impinging between the grating grooves is lost, the device works essentially as a binary amplitude grating. The pitch change during tuning is introduced by increasing the lateral gap between adjacent grating beams; therefore, the DC decreases when the structure is stretched and it increases as the device is compressed. The diffraction efficiency of the mth order as function of DC is given by [13]

$$\eta_m = \left\{\frac{\sin(2\mathrm{m}\pi * \mathrm{DC})}{2\mathrm{m}\pi}\right\}^2 + \left\{\frac{[1-\cos(2\mathrm{m}\pi * \mathrm{DC})]}{2\mathrm{m}\pi}\right\}^2. \qquad (7)$$

Due to the fact that designs with larger tunable range have larger drop in DC, they tend to suffer more loss in diffraction efficiency upon actuation. According to the simulations shown in Fig. 5, the maximum DC drop of the design at test results in negligible efficiency loss below 30 V. The loss would be more significant if a larger tunable range were desired. Analysis also shows that as long as the DC is larger than 39.8%, the first-order diffraction

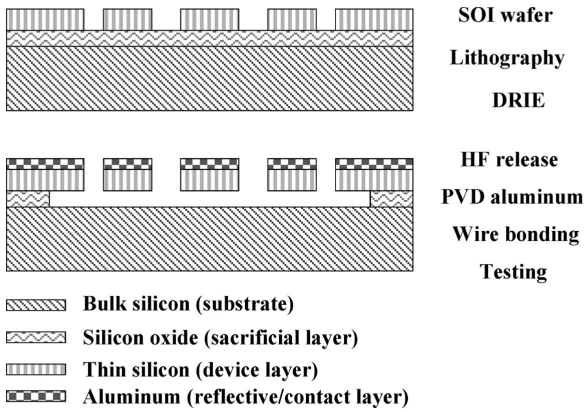

Fig. 6. Cross-sectional views of the fabrication process flow.

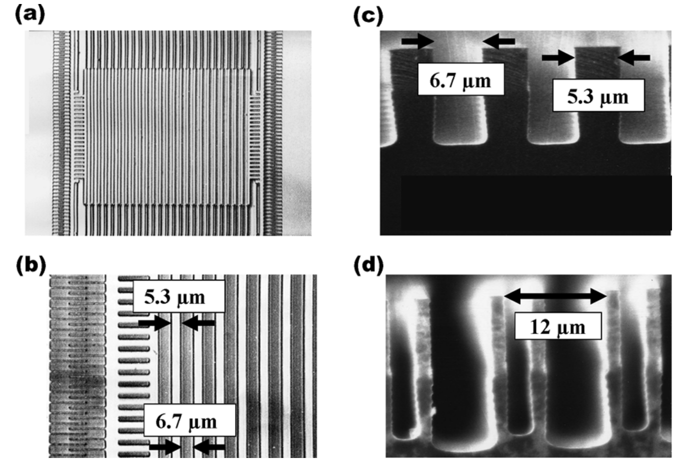

Fig. 7. (a) Optical micrograph of the device top-view. (b) Zoom-in of (a) to show the as-fabricated duty cycle. (c) SEM image of cross-sectional view of the grating beams. (d) SEM image of cross-sectional view of the flexures.

efficiency loss is less than 10% compared to the 50% DC original state. For a design with 1-μm pitch, the maximum tunable range without efficiency loss greater than 10% is 164.5 μrad.

III. Fabrication Process

Surface micromachining was first adopted to fabricate the device but our use of wet release process led to serious stiction problems. We also found that even without stiction surface micromachining results in substantial residual stress. Caution taken during multilayer deposition combined with high-temperature annealing steps might reduce the problem to a lesser degree; however, grating bowing was observed in early trials of the electrostatic device as well as the piezoelectric device [10].

To circumvent this problem, we considered using single crystal silicon substrate as the device layer. This decision eliminates the need for both thin film depositions and residual stress, hence offers great advantages such as ease of device integration and much better optical flatness. High-quality optical surface is critical for good diffraction efficiency. A rule of thumb criterion for modest surface quality is flatness better than $\lambda/10$, $\sim$50 nm in the visible wavelength range. Single crystal silicon has surface quality approaching atomic precision, therefore, the reflective coating is the major source for microscopic surface roughness in our device. On the other hand, due to the suspended nature of the grating, gravity might pull the structure down and introduce vertical sagging. However, given the high vertical stiffness and small mass of the structure, gravitational effect should be negligible. Fig. 3(b) shows excellent surface quality measured using WYKO whitelight interferometer (Veeco Instruments Inc., Woodbury, NY).

The fabrication process is depicted in Fig. 6. It starts with an SOI wafer with a 20-μm-thick device layer and a 2-μm-thick buried oxide layer. After lithography, we etch through the device layer with deep reactive ion etching (DRIE) technique (STS plc, Newport, U.K.). The advantage of using DRIE is that it allows us to obtain grating beams and flexures that are thick (20 μm) in the vertical direction with nearly 90° sidewalls. This makes high vertical stiffness possible and avoids potential stiction problems during the releasing step. The design also includes lateral bumps to ensure that no lateral stiction occurs even though the adjacent beams touch each other in the lateral dimension. During DRIE, the buried oxide layer behaves like a definite etch stop. Therefore, our design also minimizes potential problems due to loading effect (i.e., etching nonuniformity due to different exposed areas) which shows in most etching processes. The DRIE process is followed by a high-frequency (HF) etching step to release the moving parts. By designing the lateral dimension of the moving parts to be much smaller than that of the fixed parts, we have large process latitude during the time-control releasing process. After releasing, a 100-nm aluminum film is deposited by maskless thermal evaporation to form the electrodes and the reflective surface on the gratings.

The fabrication process enjoys the benefit of simplicity, since only one mask is required to define every functional element. Also, due to the fact that the only deposited layer is by thermal evaporation ($<$300 °C), the thermal budget is excellent and makes the device easy to be integrated with existing on-chip circuitry. The entire MEMS fabrication could be carried out during the back-end process of standard chip fabrication.

We fabricated several prototype gratings with the aforementioned processes. Fig. 7(a) shows the optical micrograph of the device top view. Fig. 7(b) is the zoom-in of (7a), showing the reduced DC of the fabricated device. Fig. 7(c) and (d) shows the scanning electron microscope (SEM) images of cross sectional views of a fabricated device. The measured diffraction efficiency of the first diffraction order was 9.5%, which is slightly lower than the theoretical value 10.1% for an amplitude grating with 50% on–off DC [14]. The main reason for the slightly lower diffraction efficiency is due to DRIE undercut, which made the DC drop to $\sim$44% as measured after fabrication.

IV. Device Characterization

Device characterization was conducted with two different methods: Optical beam deflection measurement and the computer microvision technique [15]. The former was done by imaging the first diffraction order using a charge-coupled device (CCD) camera and comparing centroid locations before and after actuation to determine the linear centroid movement. The angular movement was then calculated from the centroid shift divided by the focal length of the lens. The latter technique involves obtaining three-dimensional (3-D) images of

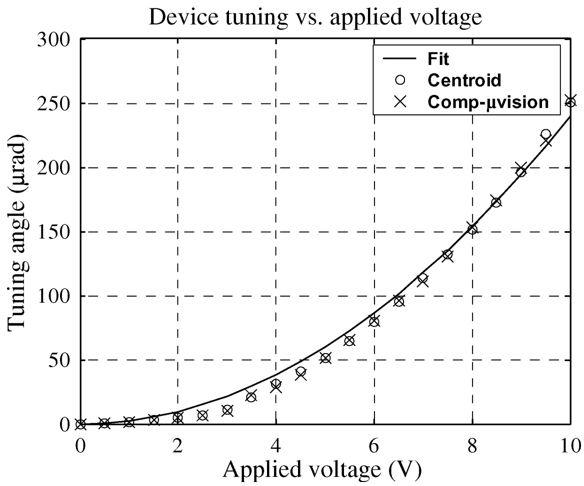

Fig. 8. Experimental results and theoretical fit of the device tuning characteristics: Angular tuning versus applied voltage. The design parameters of this prototype match those of Device 2 in Fig. 4 (summarized in Table I).

microscopic targets using the optical sectioning property of a light microscope and postprocessing the combined images to analyze the images with nanometer precision.

In Fig. 8, the centroid measurement is compared with the result from computer microvision. They are seen to be in excellent agreement with each other and also with the theory. Fitting the data with the model in (6) gives 2.399×10^{-6} for the coefficient a, which means the equivalent beam width of the flexure is $\sim$1.9 μm instead the design value of 2 μm. This agrees with the earlier observation that there was indeed DRIE undercut which made the beams narrower. The discrepancy between the fit and the data could be further explained by the nonlinear and geometry-dependent DRIE undercut [tapered and curved sidewalls in Fig. 7(c) and geometry-dependent loading effect in Fig. 7(d)], which is not accounted for by the theory. (The theory assumes uniform beam width across the entire structure.) At 10 V, we were able to tune the diffraction angle within $\sim$250 μrad. The back calculated grating pitch change is 57.4 nm, which agrees well with the computer microvision measurement of 56.9 nm at 10 V. Further tuning was attempted; however, unforeseen failure occurred and was likely due to etching debris behaving as short circuit between the input and the ground electrodes. Although we desire to pursue high resolution more than long-range tuning, a decent tunable range $\sim\mu$rad is still necessary for potential applications. In future runs, the DRIE and the releasing steps will be optimized to ensure that all residues are cleaned up before testing.

To understand the operation bandwidth of the device, we measured the frequency response using computer microvision. A generic second-order system frequency response was obtained [16] with the first resonant frequency and the damping ratio $\sim$1.4 kHz and $\sim$0.169, respectively, as shown in Fig. 9. Stability of the device was also measured by observing the centroid motion over an hour. There was no extra effort made trying to stabilize the device other than using a regulated power supply holding at 5 V. The result of Fig. 10 shows that even with no attempts of stabilization, the random fluctuation of the diffraction angle is 1 μrad (1σ) [3.28 μrad (3σ)] during over

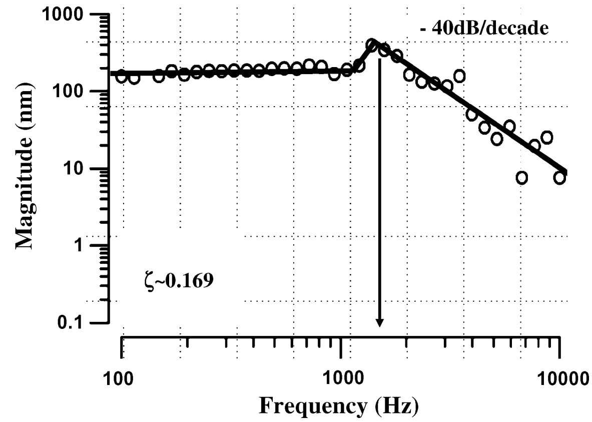

Fig. 9. Frequency response of the device measured via the computer microvision system. The first resonant frequency $\sim$1.4 kHz and damping ratio $\sim$0.169 were estimated using a standard second-order system model.

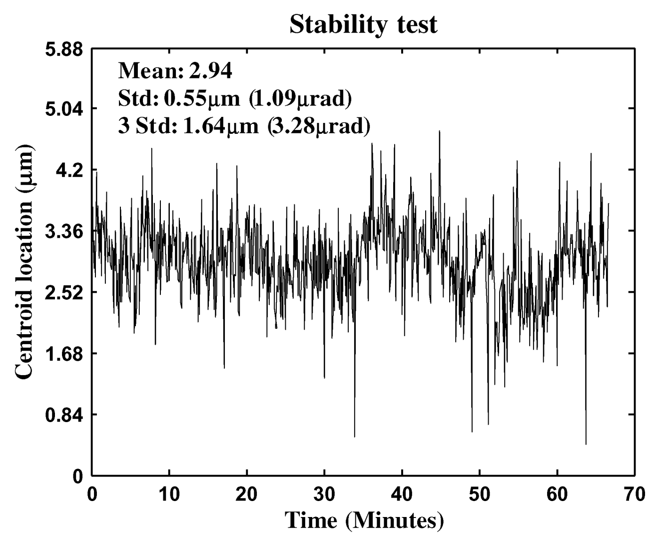

Fig. 10. Random fluctuation of the measured centroid location of the first-order diffraction beam. The device was actuated by constant voltage (5 V). Standard deviation of the centroid location was $\sim$1 μrad during over 1 h.

an hour. Potential noise sources include electronic noise in the power supply, read noise in the CCD, and random fluctuation of the compliant structure. We believe that the device angular resolution can become much better than 1 μrad after future implementation of on-chip capacitive sensing and feedback control with bidirectional comb-drives. For this specific design (12 μm/pitch), 1-μrad angular tuning corresponds to 2.28 Å in grating pitch change [see (5)].

V. Conclusion

We described the design, fabrication, and characterization of a high-resolution MEMS analog tunable grating using transverse electrostatic actuation. We have shown the device operation principles and key design parameters. Simulations of device tuning versus applied voltage performed on a particular prototype ($p_0 = 12$ μm) showed that the device could give high resolution (μrad) angular tuning. For the 1-μm-pitch grating, simulation shows that the angular tunable range could be 144 times ($\sim$30 μrad) larger than that of the current design at the same applied voltage. Further, since the tunable range quadratically depends on the applied voltage, subradian tuning could be attained in principle at higher voltage.

Diffraction efficiency loss due to grating tuning is negligible for the current design; however, it may become more significant if larger tunable range is desired. For the 1-μm-pitch design, the maximum tuning range without efficiency loss greater than 10% is 164.5 μrad. Alternatively, the device can be redesigned for operation as a transmission phase grating at wavelength range which silicon is nearly transparent, i.e., longer than 1 μm. This redesign would include a step to completely remove the substrate material below the grating.

Prototypes were fabricated using a single-mask DRIE process which requires only a single layer of thin aluminum film deposition by thermal evaporation. Therefore, minimal residual stress, excellent optical flatness, and high integration flexibility are achieved simultaneously.

Measured tuning characteristics (tuning angle against applied voltage) using two different methods agreed well with each other and also with the theory. The maximum tunable range of our first-generation device was 250 μrad with 10-V actuation, and the open-loop angular resolution was approximately 1 μrad (1σ), which can be improved with capacitive feedback control. The main reason preventing us from tuning beyond 10 V was due to etching residues. However, this is not a fundamental limit for the device. Nonlinear structural narrowing due to DRIE undercut was observed and will be accounted for in the next-generation design. The frequency response of the device was measured and peaked at $\sim$1.4 kHz, which can be made much higher after redesigning the flexure stiffness.

Given both the simulation and experimental results and the obtained experience in fabrication processes, we expect, conservatively, a next-generation device with a dynamic range of 16 b at operation voltage below 30 V. This device may be applied for applications such as thermal compensation or channel monitoring, in which diffraction efficiency requirement is not critical. In principle, by replacing the silicon grating beams with silicon nitride, a high-efficiency (40.5%) binary phase transmission grating can be realized to operate in the visible wavelength range. Another interesting application currently under investigation is the possibility of building a miniature grating spectrometer with this device, rendering optical diversity for better spectral resolution [17].

REFERENCES

[1] R. B. Apte, F. Sandejas, W. Banyai, and D. Bloom, "Deformable grating light valves for high resolution displays," presented at the Solid State Sensors and Actuators Workshop Hilton Head Island, SC, Jun. 13–16, 1994.

[2] O. Solgaard, F. S. A. Sandejas, and D. M. Bloom, "Deformable grating optical modulator," *Opt. Lett.*, vol. 17, pp. 688–690, 1992.

[3] M. B. Sinclair, M. A. Butler, A. J. Ricco, and S. D. Senturia, "Synthetic spectra: A tool for correlation spectroscopy," *Appl. Opt.*, vol. 36, pp. 3342–3348, 1997.

[4] D. E. Sene, V. M. Bright, J. H. Comtois, and J. W. Grantham, "Polysilicon micromechanical gratings for optical modulation," *Sens. Actuators A, Phys.*, vol. 57, pp. 145–151, 1996.

[5] X. M. Zhang and A. Q. Liu, "A MEMS pitch-tunable grating add/drop multiplexers," presented at the IEEE/LEOS Int. Conf. Optical MEMS, Kauai, HI, Aug. 21–24, 2000.

[6] H. Mavoori, S. Jin, R. P. Espindola, and T. A. Strasser, "Enhanced thermal and magnetic actuations for broad-range tuning of fiber Bragg grating-based reconfigurable add-drop devices," *Opt. Lett.*, vol. 24, pp. 714–716, 1999.

[7] D. M. Burns and V. M. Bright, "Development of microelectromechanical variable blaze gratings," *Sens. Actuators A, Phys.*, vol. 64, pp. 7–15, 1998.

[8] W.-C. Shih, C. W. Wong, Y. B. Jeon, S.-G. Kim, and G. Barbastathis, "Electrostatic and piezoelectric analog tunable diffractive gratings," presented at the Conf. Lasers and Electro-Optics, Long Beach, CA, May 21–26, 2002.

[9] ——, "MEMS tunable gratings with analog actuation," *Inf. Sci.*, vol. 149, pp. 31–40, 2003.

[10] C. W. Wong, Y. Jeon, G. Barbastathis, and S.-G. Kim, "Analog piezoelectric-driven tunable gratings with nanometer resolution," *J. Microelectromech. Syst.*, vol. 13, no. 6, pp. 998–1005, Dec. 2004.

[11] W. C. Tang, T.-C. H. Nguyen, and R. T. Howe, "Laterally driven polysilicon resonant microstructures," *Sens. Actuators*, vol. 20, pp. 25–32, 1989.

[12] S. D. Senturia, *Microsystem Design*. Norwell, MA: Kluwer, 2001.

[13] J. W. Goodman, *Introduction to Fourier Optics*, 2nd ed. New York: McGraw-Hill, 1996.

[14] M. Born, E. Wolf, and A. B. Bhatia, *Principles of Optics: Electromagnetic Theory of Propagation, Interference and Diffraction of Light*, 7th ed. Cambridge, U.K.: Cambridge Univ. Press, 1999, (expanded).

[15] C. Q. Davis and D. M. Freeman, "Using a light microscope to measure motions with nanometer accuracy," *Opt. Eng.*, vol. 37, pp. 1299–1304, 1998.

[16] K. Ogata, *Modern Control Engineering*, 4th ed. Englewood Cliffs, NJ: Prentice-Hall, 2002.

[17] W.-C. Shih, C. Hidrovo, S.-G. Kim, and G. Barbastathis, "Optical diversity by nanoscale actuation," presented at the IEEE Nanotechnology Conf., San Francisco, CA, Aug. 12–14, 2003.

Wei-Chuan Shih received the B.Sc. degree from the National Taiwan University, Taipei, Taiwan, in June 1997, and the M.Sc. degree from the National Chiao Tung University, Hsinchu, Taiwan, in June 1999, both in mechanical engineering. He is currently working towards the Ph.D. degree in the G. R. Harrison Spectroscopy Laboratory, Massachusetts Institute of Technology, Cambridge.

His research interests include biomedical spectroscopy and imaging, microelectromechanical systems, integrated photonics, and machine learning.

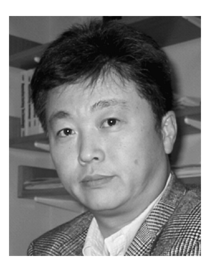

Sang-Gook Kim (M'02) received the B.S. degree from Seoul National University, Seoul, Korea, in 1978, the M.S. degree from Korea Advanced Institute of Science and Technology (KAIST), Daejeon, Korea, in 1980, and the Ph.D. degree from Massachusetts Institute of Technology (MIT), Cambridge, in 1985, all in mechanical engineering.

From 1985 to 1986, he was a Manufacturing Manager at Axiomatics Corporation, Cambridge, MA. From 1986 to 1990, he was a member of the Senior Research Staff at KAIST. Until 2003, he worked at Daewoo Corporation, Seoul, Korea, in 1991, as a General Manager at the Corporate Chairman's Office. He directed the Thinfilm Micromirror Array (TMA) Research Center, Daewoo Electronics as a Corporate Executive Director until he joined MIT in 2000 as an Associate Professor of Mechanical Engineering. At MIT, he continues his work on product realization with micro and nanoscale components. Recent research outputs include tunable microphotonic devices, self-cleaning MEMS RF switches, piezoelectric energy-harvesting MEMS, and carbon nanotube transplanting assembly.

Dr. Kim is a Member of the ASME, and a candidate member of the National Academy of Engineering of Korea and International Institution for Production Engineering Research (CIRP).

George Barbastathis (M'03) was born in Athens, Greece, on January 20, 1971. He received the Electrical and Computer Engineer's degree from the National Technical University of Athens, Athens, Greece, in April 1993, and the M.Sc. and Ph.D. degrees in electrical engineering from the California Institute of Technology, Pasadena, in June 1994 and October 1997, respectively.

After Post-Doctoral work at the University of Illinois at Urbana-Champaign, Urbana, he joined the faculty at the Massachusetts Institute of Technology (MIT), Cambridge, in March 1999, where he is currently an Associate Professor of Mechanical Engineering. His research areas are in information photonics, i.e., the use of light and optoelectronics for information processing, with emphasis on sensing, imaging, and interconnects. His research group specializes in 3-D optical systems, such as volume holograms and nonperiodic high-index contrast structures. Another area of research interest is the nanostructured origami 3-D fabrication and assembly method for constructing 3-D nanophotonic elements and other 3-D nanostructures. His past research accomplishments include the holographic method of shift multiplexing, an interferometric corneal topographer, volume holographic confocal microscopy, resonant holography, and the first-ever real-time four-dimensional (spatial and spectral) optical microscope.

Dr. Barbastathis is a member of the Optical Society of America. He is the recipient of the 3M Innovation Award (1999) and the NSF Young Investigator Award (2000), and he is presently serving as Topical Editor for the *Journal of the Optical Society of America A (Vision and Image Science)*.